Magnetic and EPR Studies of α-, β-, and γ-Fe$_2$WO$_6$ Phases at Low Temperatures

N. Guskos,† L. Sadlowski,* J. Typek,* V. Likodimos,† H. Gamari-Seale,‡ B. Bojanowski,* M. Wabia,*
J. Walczak,§ and I. Rychlowska-Himmel§

*Institute of Physics, Technical University of Szczecin, Al.Piastów 17, 70-310 Szczecin, Poland; †Solid State Section, Department of Physics, University of Athens, Panepistimiopolis, 15784 Zografou, Athens, Greece; ‡Institute of Material Science, National Research Center "Demokritos," Aghia Paraskevi Attikis, GR-15310, Athens, Greece; and §Institute of Fundamental Chemistry, Technical University of Szczecin, Al.Piastów 42, 71-065 Szczecin, Poland

The polymorphic modifications α-, β-, and γ-Fe$_2$WO$_6$ of the iron tungstate system were studied by means of magnetic susceptibility and EPR measurements at low temperatures. Both methods revealed a significant paramagnetic contribution, probably resulting from local distortions of the antiferromagnetic bulk structure induced by a disturbed cation ordering or the presence of Fe^{2+} ions. The magnetic susceptibility revealed a peak at ~260 K for all samples which can be related with an AF phase transition. The EPR spectra comprised the contribution of various isolated paramagnetic iron centers, one arising from high-spin Fe^{3+} ions in rhombic crystal field symmetry with $E/D \approx 1/3$ and $D \approx 0.22$ cm^{-1}, an anisotropic EPR signal consistent with an $S = 3/2$ ground state with large zero-field splitting, and a dominant component in the $g \approx 2$ region presumably arising from an $S = 1/2$ spin state. The latter spectra were tentatively attributed to the formation of multi-iron clusters, one of them invoking the presence of Fe^{2+} ions as well. For the β-Fe$_2$WO$_6$ phase an additional EPR spectrum was observed, which probably results from high-spin Fe^{3+} ions in a weak crystal field. © 1995 Academic Press, Inc.

INTRODUCTION

The iron–tungsten–oxygen system has been the subject of considerable interest in the research for iron-based oxide semiconductors for potential photoelectrodes, since the iron(III) tungsten Fe$_2$WO$_6$ phase was found to exhibit a relatively high conductivity ($\rho_{300\,K} \approx 50$ Ω cm) which was attributed to electron hopping between iron(III) and iron(II) sites (1). The Fe$_2$WO$_6$ system was synthesized for the first time by Kozmanov (2) from the oxidation of ferberite above 600°C. The Fe$_2$WO$_6$ oxide, prepared by heating an equimolar mixture of Fe$_2$O$_3$ and WO$_3$, was reported to crystallize in the columbite structure (3). On the other hand, Senegas and Galy (4) reported that Fe$_2$WO$_6$ crystallizes in the orthorhombic system and is the prototype of a new structural type called tri-a-PbO$_2$. Thorough studies

on iron(III) tungstate carried out by Parant *et al.* (5) have revealed the existence of two forms of Fe$_2$WO$_6$. Form I, a low-temperature modification which is obtained when prepared at temperatures below 800°C, and form II, a high-temperature modification which appears after heat treatment at temperatures above 900°C. The low-temperature phase crystallizes in the columbite structure, while the high-temperature phase in the tri-a-PbO$_2$ one. Both of these structures may be regarded as superlattice variants of the a-PbO$_2$ type (6) and the main difference between them is the nature of cation ordering. In the columbite structure, a 2:1 cation ordering of two iron and one tungsten zig-zag chains occurs, causing a tripling of the a lattice parameter, though the orthorhombic space group *Pbcn* (D_{2h}^{14}) of the a-PbO$_2$ is preserved. For the tri-α-PbO$_2$ structure, one zig-zag chain consists solely of iron ions, whereas the other two chains exhibit one-to-one ordering of iron and tungsten ions.

Recently, an investigation was undertaken in order to establish the temperature range and the heat treatment conditions which affect the synthesis of the two forms of the Fe$_2$WO$_6$ oxide (7). It has been found that in the temperature range of 750–840°C, a new polymorphic modification, which crystallizes in the monoclinic system, can be obtained. In that paper a new designation of all known modifications of Fe$_2$WO$_6$ was introduced. The low-temperature form I was denoted as α-Fe$_2$WO$_6$, the high-temperature form II as γ-Fe$_2$WO$_6$, and the newly discovered modification as β-Fe$_2$WO$_6$. This new nomenclature will be used in this paper.

The magnetic structure of γ-Fe$_2$WO$_6$ was studied by means of neutron diffraction (8, 9), while magnetic susceptibility measurements have been reported in the temperature range of 80–300 K (9) and 300–800 K (10). At low temperatures, the material is antiferromagnetic with a Néel temperature of approximately 240 K. The magnetic space group determined from the neutron scattering is *Pbc'n'*

216

and consists of ferromagnetic (100) planes coupled antiferromagnetically with spins along the [001] direction (9). Another phase transition of crystallographic character was also suggested to occur at a temperature of $T \sim 150$ K (9). Above 600 K, the inverse magnetic susceptibility was found to vary linearly with temperature with an effective magnetic moment of about 5.6 μ_B, corresponding to the spin-only moment of Fe^{3+} ions. Between 300 and 600 K the temperature dependence of the inverse magnetic susceptibility is not linear, probably due to the presence of short-range magnetic order effects.

An electron paramagnetic resonance (EPR) study of the β-Fe_2WO_6 compound at low temperatures was presented in (11). The EPR spectrum revealed the presence of at least two ion(III) centers. The first one can be attributed to Fe^{3+} ions in axial crystal field symmetry with small zero-field splitting, while the second one, which is observed at $g \approx 4.3$, was attributed to Fe^{3+} ions in the limit of full rhombic crystal field symmetry with $E/D \approx 1/3$.

As can be seen from the above, there exist a large variety of approaches for determining the magnetic and spectroscopic properties of the polymorphous group of the Fe_2WO_6 compound. Due to the growing interest in the study of the physical properties of this polymorphic system, especially in relation to the heat treatment conditions, we have studied the EPR spectra and the magnetic susceptibility for all three known phases of the Fe_2WO_6 compound, at low temperatures where there is a lack of experimental data.

EXPERIMENTAL

The preparation procedure for the three phases of the Fe_2WO_6 compound has been previously described in detail (7). The samples were identified by X-ray diffraction (XRD) using a Dron-3 X-ray diffractometer utilizing $CoK\alpha$-radiation. The XRD analysis showed that the samples of α- and γ-Fe_2WO_6 and β-Fe_2WO_6 crystallize in the orthorhombic and monoclinic crystal structures, respectively, with lattice constants similar to those in (7). All samples were found to be single phase compounds.

EPR measurements were carried out using a standard X-band ($\nu = 9.41$ GHz) spectrometer type Bruker 200D with 100 kHz magnetic field modulation. The samples, each containing 30 mg of the substance, were placed into 2-mm-diameter quartz tubes under flowing He gas in order to avoid oxygen condensation. The measurements were performed in the temperature range from 4 to 20 K using an Oxford flow cryostat system.

Magnetic measurements (dc) were performed on densely packed powder samples using a PAR 155 vibrating sample magnetometer and a SQUID type quantum design 5.5 T spectrometer. The measurements were do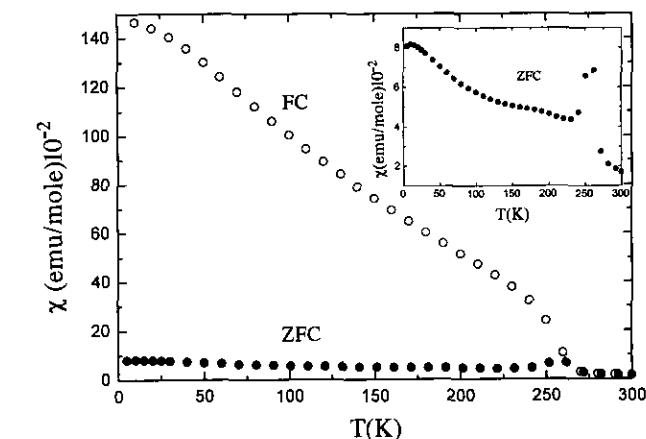ne in the temperature range from 4.2–300 K. Two modes of measurements were employed. Initially, the samples were cooled down from room temperature (RT) to 4.2 K in zero field, then a magnetic field of 0.02 T was applied and the magnetization was measured with increasing temperature (ZFC). In the second mode (FC), the sample, after being warmed, was cooled under the same magnetic field as in the ZFC mode.

RESULTS AND DISCUSSION

Magnetic Susceptibility Measurements

The temperature dependence of the static magnetic susceptibility χ for the α, β, and γ phases of Fe_2WO_6 in the temperature range of 4.2–300 K is presented in Figs. 1, 2, and 3, respectively. Samples α and γ exhibit similar behav-
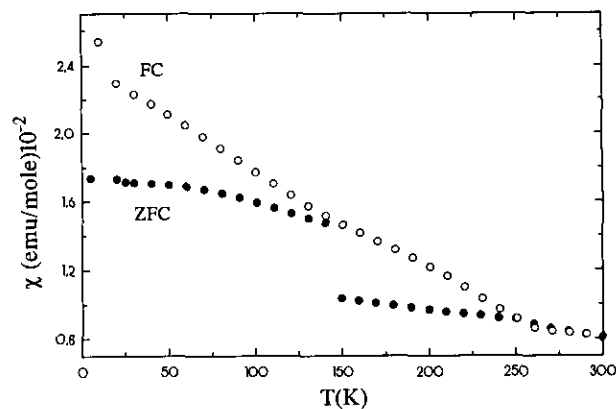

FIG. 1. Temperature dependence of the dc magnetic susceptibility for the α-Fe_2WO_6 phase in the ZFC and FC modes and in the temperature range 4.2–300 K. The inset shows the ZFC run in an expanded scale.

FIG. 2. Temperature dependence of the dc magnetic susceptibility for the β-Fe_2WO_6 phase in the ZFC and FC modes and in the temperature range 4.2–300 K.
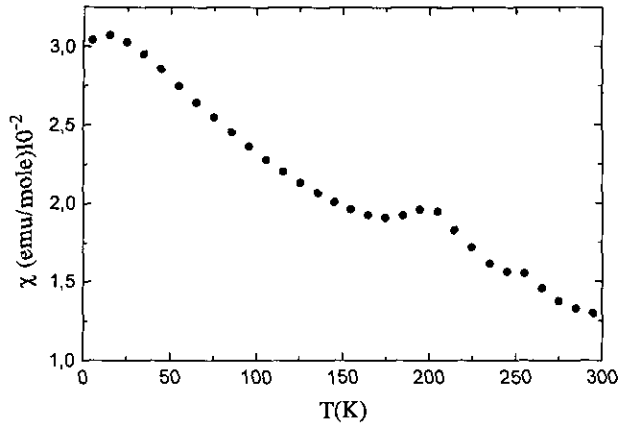
FIG. 3. Temperature dependence of the dc magnetic susceptibility for the γ-Fe_2WO_6 phase in the ZFC mode and in the temperature range 4.2–300 K.

ior (Figs. 1 and 3). Both samples in the ZFC mode exhibit a maximum at $T_1 \sim 260$ K which is more pronounced for the α phase. This peak is consistent with the antiferromagnetic phase transition detected at $T_N \sim 240$ K by neutron diffraction (8, 9). At $T_2 \sim 200$ K both samples exhibit a second peak, more pronounced in the γ phase, while upon further lowering of the temperature the susceptibility starts to increase reaching a broad maximum at a temperature $T_3 \sim 15$ K. This behavior is in contrast with the expected decrease of χ below the AF transition. The broad maximum at $T_3 \sim 15$ K is similar to the rounded susceptibility maximum χ_{max} exhibited by low-dimensional (1D or 2D) antiferromagnetic systems at temperature $T(\chi_{max})$ on the order of the exchange constant J ($k_B T(\chi_{max})/|J|$ is predicted to be approximately 10 and 18 for $S = 5/2$ Heisenberg chains and quadratic layers, respectively) (12). In the present case, such an explanation would, more likely, require the presence of antiferromagnetic iron chains with small exchange interaction of magnitude ~ 1.5 K. The maximum may also correspond to a true phase transition resulting from the incorporation of the "isolated" chains in the antiferromagnetic structure, but neutron diffraction did not provide any evidence supporting a second phase transition at low temperature (9). Additionally, the EPR parameters from such iron chains would be expected to exhibit a strong temperature dependence, while the EPR spectra described below do not show any low-dimensional behavior. Moreover, the broad maximum of the susceptibility can also originate from clusters of exchange-coupled ions, e.g., dimers of antiferromagnetically iron ions or other clusters with a suitable energy spectrum. Of course the presence of low-dimensional units cannot be excluded especially in view of the complicated structure of the compounds and the irregular behavior of χ below the AF transition temperature.

However, in the FC mode the plot changes completely (Fig. 1). The peak at 250 K is still detected but the susceptibility below that temperature increases rapidly with decreasing temperature reaching a value at 4.2 K, which is about two orders of magnitude larger than that in the ZFC run. This irreversible behavior might be related to the presence of weakly coupled clusters which, after being thermally treated under the applied magnetic field, become decoupled from the antiferromagnetic background giving rise to an enhanced paramagnetic contribution.

For the β phase a more complex behavior is observed (Fig. 2). In the ZFC run the susceptibility decreases slowly up to about 140 K and a step-like decrease is observed at about 150 K. Above this temperature, χ exhibits a small variation up to 260 K where an anomaly similar to that observed for the other phases can be detected. The same anomaly has been observed in the FC run too, though below that temperature the susceptibility started to increase rapidly as for the other phases. However, the step-like behavior at 150 K was not seen in the FC mode. The 150-K anomaly is close to the one observed by Pinto et al. (9), who suggested the presence of a transition of crystallographic origin due to a shift of the ionic positions.

In order to account for the behavior of χ for the three phases of Fe_2WO_6, we suggest that the observed magnetic susceptibility is the result of a dominant antiferromagnetic component which gives rise to the small values of χ at low temperatures, and a "paramagnetic" contribution resulting from clusters of exchange coupled iron ions or even isolated iron(III) ions taken in different proportion for each phase. One can speculate that the strength of this paramagnetic contribution is proportional to the magnitude of the presumed disorder in the iron–tungsten zig-zag chains along the c-axis (4). The various temperatures obtained for the three phases are summarized in Table 1 together with magnetic data previously reported.

Electron Paramagnetic Resonance

The EPR spectra recorded at low temperatures for the α-, β-, and γ-Fe_2WO_6 phases turn out to be rather compli-

TABLE 1

The Critical Temperatures for the Various Fe_2WO_6 Phases as Defined in the Text

Phase	T_1 (K)	T_2 (K)	T_3 (K)	Reference
α	260	~200	~15	This work
β	260	—	—	This work
γ	240	~220	—	(9)
	260	~200	~15	This work

Note. The temperature T_1 corresponds to the T_N.
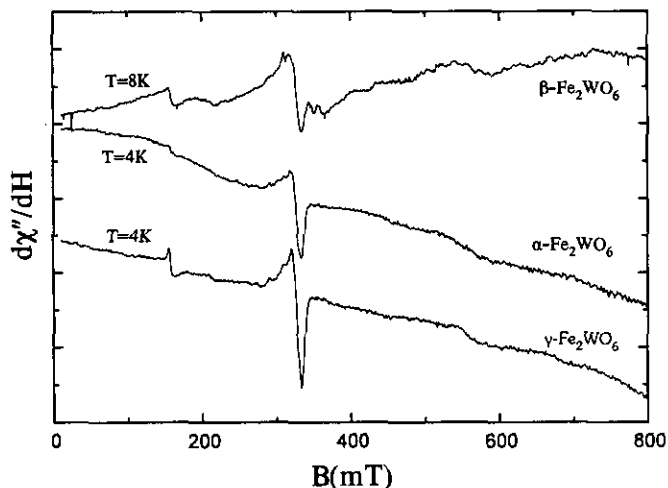
FIG. 4. The EPR spectra of the α-, β-, and γ-Fe$_2$WO$_6$ phases at low temperatures.

cated as shown in Fig. 4. However, two relatively intense resonance spectra, in the $g \approx 2.0$ and $g \approx 4.3$ regions, superimposed on the background of a very broad line spreading beyond the range of the applied magnetic field, are observed for all samples. Moreover, many weak resonance lines are observed in different parts of the spectra. The low-field EPR spectrum centered at $g \approx 4.3$ is characteristic of high-spin Fe^{3+} ions in a crystal field of extreme rhombic symmetry. Due to the relatively narrow linewidth of these lines, we conclude that the underlying iron centers should be magnetically isolated from the bulk antiferromagnetic structure existing at low temperatures in Fe$_2$WO$_6$. On the other hand, the broad background line must be associated with iron(III) ions incorporated in the bulk magnetic structure, where the strong antiferromagnetic correlations result in an excessive broadening of the resonance signal.

Figure 5 presents the EPR spectrum of the γ-Fe$_2$WO$_6$ phase at some selected temperatures. As can be seen, additional powder lines were resolved in the $g \approx 4.3$ region at higher temperatures, especially at $T = 15$ K. As well known, an adequate spin Hamiltonian which describes the $g \approx 4.3$ spectrum of high-spin Fe^{3+} ($^6S_{5/2}$) ions assumes the form

$$H = g\beta \mathbf{H} \cdot \mathbf{S} + D\left[S_z^2 - \frac{S}{3}(S + 1)\right] + E(S_x^2 - S_y^2), \quad [1]$$

where g is the electronic g-factor, assumed to be isotropic, β is the Bohr magneton, while D and E are the axial and the rhombic crystal field parameters, respectively. Diagonalization of the above spin Hamiltonian in the weak magnetic field limit, $|D|$, $|E| \gg g\beta H$, yields three Kramers

doublets in zero magnetic field. The $g \approx 4.3$ spectrum is associated with the transitions within the middle Kramers doublet in the case of a strong crystal field $|D| \gg g\beta H$, and a maximum degree of rhombic distortion, corresponding to $\lambda = E/D \approx 1/3$. Calculations of the powder EPR spectrum of high-spin Fe^{3+} ions showed that this spectrum can exhibit a fine structure, which may comprise up to six powder lines resulting from transitions with the magnetic field along the principal x, y, z axes as well as along the principal xy, yz, xz planes (13). Frequently, these lines average, resulting in the anisotropic lineshape of the $g \approx 4.3$ powder spectrum, as it occurs for the present EPR spectra for most temperatures (Fig. 5). Assuming that the powder lines at $g \approx 4.03$ and $g \approx 4.13$, most clearly resolved at $T = 15$ K, arise from this kind of spectrum and using the diagrams reported by Aasa (13), we find that the observed EPR spectrum at $g \approx 4.3$ consists of five components with $D \approx 0.22$ cm^{-1} and $E/D = 0.32$. The other powder lines are predicted to occur at $g = 4.34$, $g = 3.96$, and $g = 3.90$, the first two being easily detected at $T = 15$ K, while the third one might be rather weak to be observed. The $g \approx 4.3$ spectrum can be seen in more detail in Fig. 6, at $T = 15$ K where the spectrum is clearly resolved, along with the predicted positions of the powder lines and at $T = 14$ K where the fine structure details are obscured. This assignment is also supported by the presence of two broad humps at higher magnetic fields, $\sim$580 mT and $\sim$680 mT (Fig. 4), which are predicted to occur from transitions between the other energy levels of the Fe^{3+} ions for the same values of D and E (13). Additional weak powder lines are expected in the $g \approx 2$ region, probably contributing in the complex structure of the observed EPR spectrum at this region (Fig. 5).

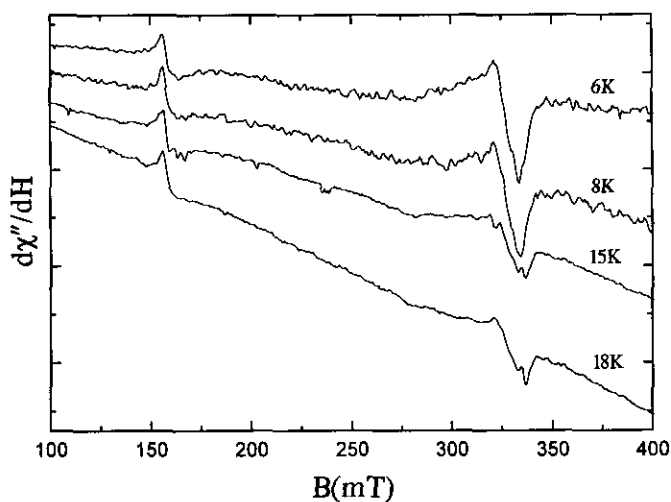According to this assignment, another contribution at

FIG. 5. The EPR spectra of the γ-Fe$_2$WO$_6$ phase at different temperatures.
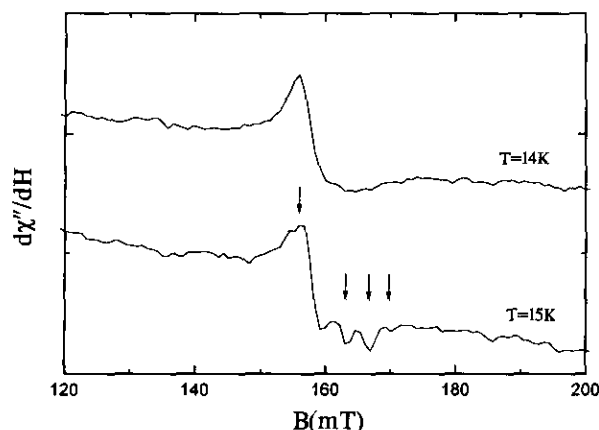
FIG. 6. The EPR spectrum of the γ-Fe$_2$WO$_6$ phase in the $g \approx 4.3$ region at $T = 14$ K and $T = 15$ K. The arrows indicate the predicted powder line positions for the values of D and E reported in the text.

$g \approx 4.25$ would be expected to account for the observed spectrum in this region, as can be easily seen from Fig. 6. An additional indication for such a contribution arises from the small temperature dependence of the intensity of the $g \approx 4.3$ spectrum under nonsaturation conditions, which is very small compared to the calculated temperature variation of the EPR spectrum intensity using the estimated values of D and E. Figure 7 presents the temperature variation of the spectrum's amplitude in comparison with the calculated temperature dependence which is dominated by the Boltzman population of the middle Kramers doublet. From Fig. 5, it is also seen that a sharp powder line centered at $g = 1.998(1)$ is gradually resolved at higher temperatures, while another broad resonance line is observed at 210 mT with $g_{eff} \approx 3.2$ (Fig. 4). This kind of
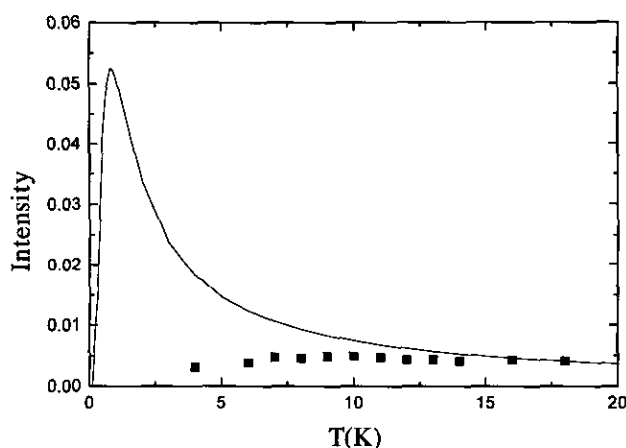

FIG. 7. The temperature dependence of the amplitude of the $g \approx 4.3$ spectrum normalized to the calculated temperature variation of the EPR intensity. The squares correspond to the experimental points and the solid line to the calculated intensity.

powder pattern with effective g values of 4.25, 3.2, and 1.998 is typical of an $S = 3/2$ spin system with large zero field splitting. Such an EPR spectrum has been frequently identified in the iron–molybdenum protein of the enzyme nitrogenase, as well as in various synthetic model compounds of the formula [Fe(MS$_4$)$_2$]$^{3-}$ (M = Mo, W) or clusters of the type MF$_3$S$_4$ (M = Mo, W) (14–16). The corresponding spin Hamiltonian has the form [1] with an anisotropic g tensor and in the absence of an external magnetic field gives rise to two Kramers doublets separated in energy by $\Delta = 2|D|(1 + 3\lambda^2)$, where D and λ have their usual meaning (17). In the case of large zero field splitting, the lowest Kramers doublet with $m_s = \pm 1/2$ gives rise to an extremely anisotropic powder spectrum which can be described by a fictitious spin $S' = 1/2$ with principal values $g_{x'}$, $g_{y'}$, and $g_{z'}$ given by the relations (14, 16)

$$g_{y,x'} = g_\perp \left[1 + \frac{1 \pm 3\lambda}{(1 + 3\lambda^2)^{1/2}} \right]$$

$$\text{and} \quad g_{z'} = g_\parallel \left[\frac{2}{(1 + 3\lambda^2)^{1/2}} - 1 \right]. \quad [2]$$

Using the values $g_{x'} = 3.2$, $g_{y'} = 4.25$, $g_{z'} = 1.998$, and the above equations, we obtain $g_\perp \approx g_\parallel \approx 2.0$ and $\lambda = 0.09$. The latter value indicates a small rhombic distortion. The origin of the $S = 3/2$ spin state is not easily explained on the basis of the formal oxidation states of the existing metals in the Fe$_2$WO$_6$ compounds, namely the high-spin Fe^{3+} ($S = 5/2$) and the diamagnetic W^{6+} ions. The presence of an $S = 3/2$ state could be in principle explained by the presence of the rarely observed Fe$^+$ ($S = 3/2$) ions or by the presence of W^{5+} ($5d^1$, $S = 1/2$) ions with two of them being antiferromagnetically coupled to one iron Fe^{3+} ($S = 5/2$) ion to produce an $S = 3/2$ ground state, though neither of these alternatives appears to be probable since there is no evidence corroborating such valence states of the metal atoms. However, Sieber et al. (1), in order to account for the semiconducting behavior of the Fe$_2$WO$_6$ compound, have suggested the presence of Fe^{2+} ($3d^2$, $S = 2$) ions due to a solid solution of a small amount of FeWO$_4$ in Fe$_2$WO$_6$, while recent ^{57}Fe Mossbauer studies of the iron tungstate oxides, though they favor the dominant contribution of the Fe^{3+} ions, do not exclude the possibility of a small amount of reduced Fe^{2+} ions (18). Allowing for the presence of a small number of Fe^{2+} ions, the $S = 3/2$ spin state may originate as the ground state of a three iron cluster comprising two ferromagnetically coupled Fe^{2+} ions which are antiferromagnetically coupled to one Fe^{3+} ion.

As can be seen from Figs. 4 and 5 the observed EPR spectrum in the $g \approx 2$ region, at least for the α- and γ-Fe$_2$WO$_6$ phases, resembles closely the powder pattern of an $S = 1/2$ spin system. However, a computer simulation of this spectrum for the usual $S = 1/2$ spin Hamiltonian
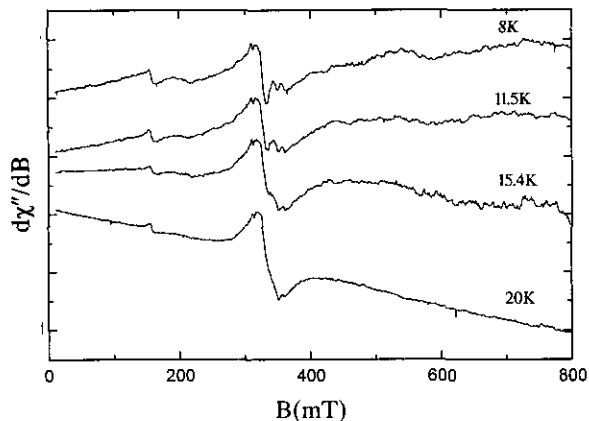
FIG. 8. The EPR spectra of the β-Fe$_2$WO$_6$ phase at different temperatures.

was not successful, since we could not unambiguously identify the relevant powder lines due to the presence of other contributions as described above. An $S = 1/2$ spin state might arise from the antiferromagnetic coupling of one high spin Fe^{3+} ($S = 5/2$) with one Fe^{2+} ($S = 2$) ion as previously reported for an [2Fe–2S] ferredoxin (19). Another more likely interpretation which does not require the presence of Fe^{2+} ions is the formation of a three-iron cluster containing three antiferromagnetically coupled high-spin Fe^{3+} ions. In this case, the spin Hamiltonian describing the isotropic exchange interaction between three $S = 5/2$ paramagnetic centers in the form of a general triad is given by

$$H_{ex} = J_{12}\,\mathbf{S_1} \cdot \mathbf{S_2} + J_{13}\,\mathbf{S_1} \cdot \mathbf{S_3} + J_{23}\,\mathbf{S_2} \cdot \mathbf{S_3}, \qquad [3]$$

where J_{12}, J_{13}, and J_{23} are the exchange coupling constants, which in the general case are different. In the case of a symmetric triad ($J_{13} = J_{23}$) and antiferromagnetic exchange interactions, one of the two possible states with total spin $S = 1/2$ becomes the ground state of the cluster when the ratio $x = J_{13}/J_{12}$ of the exchange coupling constants lies in the range $0.6 \leq x \leq 1.8$ (20). In the general case, the $S = 1/2$ ground state is stabilized provided that the exchange coupling constants are not very different, $J_{12} \approx J_{13} \approx J_{23}$. The presence of a cluster of this type in Fe$_2$WO$_6$ may be related to a disordered distribution of the Fe and W atoms, disturbing the long-range antiferromagnetic ordering and giving rise to isolated iron clusters.

Figure 8 presents the EPR spectrum of the β-Fe$_2$WO$_6$ phase at different temperatures. As can be seen, the spectrum exhibits the same powder patterns that were identified in the γ-Fe$_2$WO$_6$ phase, namely the $g \approx 4.3$ spectrum along with the high-field (580 and 700 mT) lines, the three-line $S = 3/2$ powder spectrum, and a dominant contribution of presumably an $S = 1/2$ spin system in the $g \approx 2$ region.

However, two additional absorption-type powder lines are observed at 350 and 365 mT and a sharp peak at 311 mT, while the structure of the central line is more complicated than the other samples. Assuming that this additional EPR spectrum comprises only lines in the central $g \approx 2$ region, it can be interpreted in terms of isolated Fe^{3+} ions under the action of a weak crystal field, so that the crystal field parameters D and E are much smaller than the Zeeman energy $g\beta H$. In this case, the single crystal EPR spectrum consists of five resonance lines, each giving rise to two or three powder lines in the case of axial or rhombic symmetry, respectively, besides the central $+1/2 \leftrightarrow -1/2$ transition which may be split in three to six powder lines for axial or rhombic crystal field symmetry (13, 21). Taking into account the small spread ($\sim$60 mT) of the observed powder lines around $g = 2$, where the central line is expected, we make a rough estimate of the axial crystal field parameter of $D \approx 0.007$ cm^{-1}. The observation of such a spectrum may indicate the presence of isolated octahedrally coordinated Fe^{3+} ions with a small axial/rhombic distortion in the β-Fe$_2$WO$_6$ phase.

The α-Fe$_2$WO$_6$ phase exhibited EPR spectra that were very similar to those observed for the γ-phase (Fig. 3). The intensity of the EPR spectra was smaller for both the $g \approx 4.3$ spectrum and the $g \approx 2$ EPR lines in comparison with the other phases, inhibiting a more detailed analysis. The relatively strong intensity of the broad background line (Fig. 4) as well as the intense peak at 260 K of the magnetic susceptibility (inset Fig. 1) indicate the presence of a dominant antiferromagnetic contribution.

Finally, we would like to note that the described assignments of the different EPR spectra should be considered as tentative ones, since the poor resolution of the observed powder spectra does not allow an unambiguous identification of the various lines. In this respect, EPR measurements at higher frequencies may enable a better resolution of the EPR spectra so that accurate simulations of the various paramagnetic centers would be performed, while EPR measurements at high temperatures ($T > 260$ K), which are currently in progress, will reveal the EPR response of the bulk Fe ions and the critical behavior expected near the antiferromagnetic phase transition. The EPR results

TABLE 2
The Zero Field Splitting Parameters for the Various EPR Spectra Described in the Text

Spin S	D (cm^{-1})	$\lambda = E/D$	Phase	Reference
5/2	0.22	0.32	α, β, γ	(11), This work
5/2	$\sim$0.007	—	β	(11), This work
3/2	>0.3	0.09	α, β, γ	This work
1/2	—	—	α, β, γ	This work

obtained in this and previous works are summarized in Table 2.

It should also be noticed that the trimeric models proposed to explain the observed $S = 3/2$ and $S = 1/2$ EPR spectra are the simplest ones, since single ions or dimers of iron(III) cannot produce such ground states. However, larger exchange-coupled units with different exchange coupling constants, resulting from a statistical distribution of iron atoms, may probably give rise to these ground states (22) but still such an assignment would be on a rather arbitrary basis. In this respect, the proposed trimeric units should be considered as tentative ones.

CONCLUSIONS

Magnetic susceptibility and EPR measurements of the α-, β-, and γ-Fe_2WO_6 phases at low temperatures revealed, besides the expected antiferromagnetic component due to the magnetic ordered state at higher temperatures, the presence of a considerable paramagnetic contribution in the magnetic response of the compounds. A peak in the susceptibility at $T_1 \sim 260$ K can be related with an AF phase transition previously identified by neutron diffraction (9). The EPR spectra exhibited the presence of various paramagnetic iron centers, which were tentatively attributed to the existence of two kinds of isolated Fe^{3+} ions in a moderate and weak crystal field of low symmetry, respectively, and to the formation of iron clusters producing ground states with $S = 1/2$ and $S = 3/2$ total spin. It is suggested that a disordered state in the cation ordering of Fe and W atoms, as well as the presence of Fe^{2+} ions, may locally frustrate the antiferomagnetically ordered structure, inducing the formation of different paramagnetic iron species unassociated from the bulk of the compound.

REFERENCES

1. K. Sieber, H. Leiva, K. Kourtakis, R. Kershaw, K. Dwight, and A. Wold, *J. Solid State Chem.* **47**, 361 (1983).
2. Yu. D. Kozmanov, *Zh. Fiz. Khim.* **31**, 1861 (1957).
3. G. Bayer, *Ber. Dtsch. Keram. Ges.* **39**, 535 (1962).
4. J. Senegas and J. Galy, *J. Solid State Chem.* **10**, 5 (1974).
5. C. Parant, J. C. Bernier, and A. Michel, *C. R. Acad. Sci. Paris Ser. C* **276**, 495 (1973).
6. H. Leiva, K. Sieber, B. Khazai, K. Dwight, and A. Wold, *J. Solid State Chem.* **44**, 113 (1982).
7. J. Walczak, I. Rychlowska-Himmel, and P. Tabero, *J. Mater. Sci.* **27**, 3680 (1992).
8. H. Weitzel, *Acta Crystallogr. Sect. A* **32**, 592 (1976).
9. H. Pinto, M. Melamud, and H. Shaked, *Acta Crystallogr. Sect. A* **33**, 663 (1977).
10. H. Leiva, R. Kershaw, K. Dwight, and A. Wald, *J. Solid State Chem.* **47**, 293 (1983).
11. L. Sadlowski, N. Guskos, V. Likodimos, B. Bojanowski, M. Wabia, J. Typek, J. Walczak, and I. Rychlowska, *Proc. Cong. Ampere, 28th, 1994.*
12. L. J. De Jongh and A. R. Miedema, *Adv. Phys.* **23**, 1 (1974).
13. R. Aasa, *J. Chem. Phys.* **52**, 3919 (1970).
14. R. A. Venters, M. J. Nelson, P. A. McLean, A. N. True, M. A. Levy, B. M. Hoffman, and W. H. Orme-Johnson, *J. Am. Chem. Soc.* **108**, 3487 (1986).
15. P. K. Mascharak, G. C. Papaefthymiou, W. H. Armstrong, S. Foner, R. B. Frankel, and R. H. Holm, *Inorg. Chem.* **22**, 2851 (1983).
16. G. D. Friesen, J. W. McDonald, W. E. Newton, W. B. Euler, and B. M. Hoffman, *Inorg. Chem.* **22**, 2202 (1983).
17. J. R. Pilbrow, "Transition Ion Electron Paramagnetic Resonance." Clarendon Press, Oxford, 1990.
18. T. Birchall, C. Hallet, A. Vaillancourt, and K. Ruebenbauer, *Can. J. Chem.* **66**, 698 (1988).
19. J. F. Gibson, D. O. Hall, J. H. M. Thornley, and F. R. Whatley, *Proc. Natl. Acad. Sci. U.S.A.* **56**, 987 (1966).
20. J.-J. Girerd, G. C. Papeefthymiou, A. D. Watson, E. Gamp, K. S. Hagen, N. Edelstein, R. B. Frankel, and R. H. Holm, *J. Am. Chem. Soc.* **106**, 5941 (1984).
21. R. Odermatt, *Helv. Phys. Acta* **54**, 1 (1981).
22. E. Belorizky, *J. Phys. I* **3**, 423 (1993).